CHEMISTRY OF MATERIALS
Review

Chem. Mater. **XXXX,** *XXX,* 000–000 A
DOI:10.1021/cm102144h

Photoconducting Polymers for Photorefractive 3D Display Applications†

Jayan Thomas,*,‡ Cory W. Christenson,‡ Pierre-Alexandre Blanche,‡ Michiharu Yamamoto,§ Robert A. Norwood,‡ and Nasser Peyghambarian‡

‡*College of Optical Sciences, The University of Arizona, Tucson, Arizona 85721, United States, and* §*Nitto Denko Technical Corporation, Oceanside, California 92054, United States*

Received July 30, 2010. Revised Manuscript Received October 23, 2010

Photorefractive composites derived from photoconducting polymers offer the advantage of dynamically recording holograms without the need for processing of any kind. Thus, they are the material of choice for many cutting edge applications, such as updatable 3D displays and imaging through a scattering medium. This article reviews the basic properties of photorefractive polymer systems and the inherent advantages that have attracted much attention. The chemistry and physics relevant for the design of the high-performance guest−host composite are discussed and recent advances emphasized. In particular, a charge transporting polymer with high mobility and history-independent response times is highlighted, as well as polymer systems useful for holographic displays and the material considerations necessary to develop high-speed, large-sensitivity composites.

Introduction

Photorefractive (PR) polymers have advanced quickly since their initial discovery in 1991,[1] and now perform with high efficiencies and fast response times.[2−4] The PR effect, originally discovered in inorganic crystals more than 40 years ago,[5,6] initially drew attention as a perceived detriment to nonlinear applications in these materials. However, development was pursued because of some unique properties relevant to other perceived applications. First, the process was reversible though also fixable,[7] allowing both read/write and read-only applications, as opposed to standard photographic films which could only be written once. Second, the nonlocal nature of the process allowed coupling and energy transfer to occur between two coherent beams.[8] Even though there have been tremendous advancements in the materials, these are still among the primary reasons photorefractives are pursued as the material of choice for many areas.

When the effect was discovered in organic polymers, a number of advantages over inorganics were soon realized. Organic polymer materials have the inherent advantages of ready manipulation of component formulations to suit a given application and low cost. The structural constraints were also relaxed, allowing them to be custom-made into different geometries, such as waveguides and displays; significantly, samples can be made much larger than is typical for crystals. The dielectric constant is also smaller, which reduces the electric field screening of trapped charges and increases the quality factor. The highly customizable doping process, where specific atoms or molecules are added to control the electrical conductivity, optical nonlinearities, or charge trapping properites, is also easier compared to crystals, where dopants are typically expelled during growth. The drawbacks are that they are more dispersive in nature, both optically and electronically, and the mechanism behind their operation is significantly more complicated than regular crystals, though much work has been done in these areas.[9,10] PR polymers now outperform inorganic counterparts in diffraction efficiency, two-beam coupling gain, and sensitivity.[2,11,12]

Because of this tremendous progress, many applications have appeared,[13] including optical communication,[14] correlation,[15] and imaging through scattering media,[16−18] all with different material challenges that can be met by these highly versatile polymers. Recently, they have been shown to function in dynamic holographic displays,[19] which are of use in medical imaging, industrial design, defense applications, and air traffic control, among other emerging areas such as 3D telepresence. Unlike other permanent media for recording holograms, PR polymers are reversible and require no postprocessing. They demonstrate fast response time, long persistence, and high diffraction efficiency, which are necessary material properties for such an application. However, progress in other areas has not been as rapid, particularly in the area of sensitivity. In the visible, the sensitivity is still orders of magnitude smaller than that of permanent films used for recording static holograms. There are also few routes to extend operation into the infrared (IR), and only recently have these begun to bear fruit. Some of these include using organic photosensitizers with one photon absorption in the near IR,[20,21] using semiconductor nanocrystals where the absorption band is tunable,[22] and using two-photon absorption to charge sensitizers that are otherwise transparent.[23] So few organic molecules undergo transitions in the IR that two-photon absorption

† Accepted as part of the "Special Issue on π-Functional Materials".

*Corresponding author. E-mail: jthomas@optics.arizona.edu.

(TPA) has been used, and while more difficult experimentally, provides several advantages such as nondestructive read out.[24]

This article reviews the basic material concepts behind fabrication of organic PR polymer composites, including the functional components, their respective roles in devices, and the basic physical mechanisms that must be taken into account when designing devices. Recent progress in these areas is also discussed, including new hole-transporting polymers for reduced glass transition temperature (T_g) and high mobility. Particularly, a bis-triarylamine side-chain host polymer exhibits less deep trapping leading to stable dynamics independent of the illumination history. Many novel sensitizers are also reviewed, which is a very dynamic area of research. New composites with excellent sensitivity in the near IR wavelengths have extended the range of high-performing polymers beyond the visible. Finally, some material considerations necessary for specific applications are also taken into account, such as pulsed writing for high speed operation of many devices, and updatable holographic displays. Optimized materials have been shown to exhibit good performance even under single pulse nanosecond writing times, enabling operation at 100 Hz or more, which is faster than CW recording schemes. The materials for holographic displays are discussed and extensions to reflection geometry and video-rate response times are examined, because still higher sensitivities and trap densities are needed to accomplish these goals.

Photorefractivity

In photorefractive materials, a three-dimensional refractive index modulation is induced by a nonuniform illumination. When two coherent beams intersect within the photorefractive material, a spatially modulated intensity pattern is produced which is given by[11]

$$I(x) = I_0[1 + m\cos(2\pi/\Lambda)] \quad (1)$$

where $I_0 = I_1 + I_2$ is the total incident intensity, i.e., the sum of the intensities of the two beams; $m = 2(I_1 I_2)^{1/2}/(I_1 + I_2)$ the fringe visibility and Λ the spatial wavelength or periodicity. In a tilted transmission geometry Λ is given by

$$\Lambda = \frac{\lambda}{2n\sin[(\alpha_2 - \alpha_1)/2]} \quad (2)$$

where n is refractive index of the material, λ the optical wavelength in vacuum, and α_1 and α_2 the incident internal angles of the two writing beams relative to the sample normal. Λ determines the period of the sinusoidal light distribution, which can vary from a fraction of a micrometer to a couple of tens of micrometers with writing beams at visible optical wavelengths. The intersecting beams produce an interference pattern within the material and charge carriers are generated in the high intensity regions. Since the mobility of the majority carriers (usually holes in organic materials) are higher, they move from the high intensity region, leaving behind the carriers of opposite charge, and

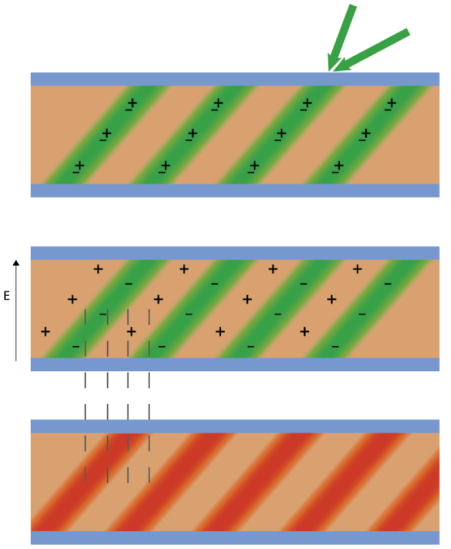

Figure 1. Schematic diagram showing the steps involved in the photorefractive process. In the top panel, the writing beams interfere, creating an interference pattern and generating electron−hole pairs in the bright regions. In the middle, the charges separate under the influence of an external electric field, which leads to a similar space-charge field and index modulation, shown together at the bottom since they are in phase. Note that the antinode of the modulation occurs at the node of the interference because of the charge separation.

get trapped in the dark region. The driving force for the charge carriers is either diffusion due to a concentration gradient present in the medium or drift if an external electric field is applied (generally the case for organic materials). The traps present in the material limit the migration process, which can take place on micrometer length scales. Charges trapped in low intensity regions and those opposite charges left behind in high intensity regions give rise to an inhomogeneous space charge distribution. A schematic of the charge generation, transport, trapping and space charge field generation is depicted in Figure 1. As given in (1), for a one-dimensional light intensity distribution, a space charge distribution $\rho(x)$ in a material with a dielectric constant ε induces an internal space charge field $E_{sc}(x)$ by Poisson's equation, which is $dE_{sc}/dx = 4\pi\rho/\varepsilon$. If the transport is governed by diffusion alone, the phase shift between the space charge field and the light intensity distribution is $\pi/2$, otherwise it depends on the relative strength of the diffusion and drift processes. The final step in the photorefractive grating formation is the electro-optic (EO) modulation of the refractive index of the material by the internal space charge field. The phase-shift that occurs as a result of the dephasing between the initial light distribution and the refractive index modulation is the fingerprint of photorefractivity.[25] A diagram of the typical sample geometry used in most cases to characterize PR polymers is shown in Figure 2.

Among the metrics commonly used to quantify the performance of PR polymers, diffraction efficiency and two-beam coupling (TBC) gain will be discussed extensively here. Diffraction efficiency is defined as the light power in a single diffracted order divided by either the light incident on the device (external efficiency) or the light transmitted through the sample without a grating

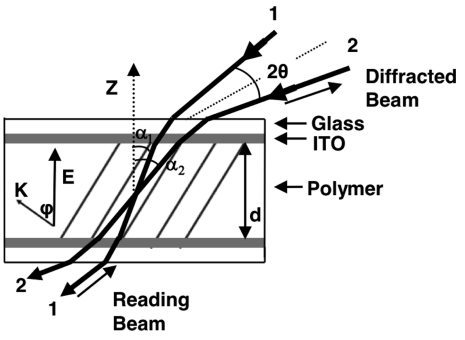

Figure 2. Typical geometry for testing the photorefractive properties of a polymer. In transmission, two writing beams (1 and 2) are incident from the same side with an angle between the sample normal and bisector usually between 50 and 70°. To probe the diffraction efficiency, a reading beam is made to counter-propagate with one of the writing beams. *E* is the applied DC field, *d* is the sample thickness, and *K* is the grating vector.

present (internal efficiency). The gratings are usually thick enough (Bragg regime) so that only one diffracted order is present. This is measured in a four-wave mixing (FWM) setup where two writing beams are incident on the sample while a weak reading beam is sent counter-propagating to one of the writing beams. The steady-state efficiency is measured by monitoring the transmitted and diffracted orders while slowly increasing the applied field. The transient efficiency is measured by applying a constant field and monitoring the beams over time.

In TBC, two writing beams are incident in the material and will each diffract from the grating they themselves created, with one beam experiencing more diffraction than the other. This leads to an increase in the intensity of one beam at the loss of the other. The magnitude of this energy transfer is characterized by the TBC gain parameter Γ and can be calculated using

$$\Gamma = \frac{1}{d}(\cos\alpha_1 \ln\gamma_1 - \cos\alpha_2 \ln\gamma_2) \qquad (3)$$

where d is the material thickness, α_1 and α_2 are the angles of beam 1 and 2 inside the sample, and γ_1 is the intensity of beam 1 with beam 2 present divided by the intensity of beam 1 with beam 2 off (and similarly for γ_2). TBC is considered as a signature of the PR effect because TBC gain will only be observed for a nonlocal grating arising from the phase shift between the space charge field and the optical interference pattern. More details on these and other PR measurements can be found elsewhere.[4]

Orientational Enhancement

It was observed early on that the performance of PR polymers was far greater than what could be predicted based on the standard model for crystals, where the index modulation has its origin in the linear electro-optic (EO) effect ($\chi^{(2)}$). In a study by Moerner et al.,[26] it was discovered that a different mechanism was primarily responsible for the change in the index of refraction in photorefractive polymers, and was dubbed "orientational enhancement." This is a very important aspect of the physics of the PR effect in polymers, especially with respect to guiding material developments.

In inorganic crystals, the index modulation is provided by the linear EO or Pockels effect, which arises from the hyperpolarizability and leads to an electric-field induced changes in the refractive index. The Pockels effect only exists in crystals that are noncentrosymmetric, hence in ferroelectric crystals like lithium niobate or barium titanate, the crystal domains must first be aligned by applying a poling field. In polymers with a T_g near room temperature, a noncentrosymmetry is achieved by applying a DC field, which orient nonlinear optical (NLO) chromophores via interaction of the dipole moment with the field, creating a macroscopic orientation of the dipoles. However, it was discovered that they could also be oriented in situ to the spatially varying space-charge (SC) field created by the trapping of the photogenerated charges. Thus, the anisotropy in the linear polarizability of the molecules will also lead to a macroscopic index modulation. In polymers, this has a much larger effect on the performance than the hyperpolarizability.

To be most effective, the poling should be performed at or above the T_g of the material, and various methods can be taken to decrease the T_g, such as addition of plasticizers to the composite. When the field is turned off, the chromophore orientation will cease to be organized and the index modulation will be lost. The orientation will be quasi-permanent if the T_g is above the operating temperature, but in this case the initial alignment will take longer. This has led to various methods to counter-act this trade-off, such as thermal fixing.[27] During the writing of a grating, the interfering beams of light will produce the SC field, which is added vectorially to the applied electric field. The chromophores will orient to this total electric field if the T_g is low enough, resulting in a complex spatial dependence of the dipoles.

PR Polymer Components

In a typical PR guest−host system, a hole-transporting polymer matrix is doped with a photoreducible molecule (photosensitizer) that can either absorb light or form a charge-transfer complex with the hole-transport polymer. Upon excitation of an electron from the highest occupied molecular orbital (HOMO) to the lowest unoccupied molecular orbital (LUMO) of photosensitizer, a hole is injected into the transport system which becomes trapped and a NLO chromophore subsequently produces the field-dependent refractive index as discussed above. The magnitude and speed of the charge generation, injection, transport, and trapping depends on the relative values of the HOMO and LUMO levels of each component, as discussed below. As the highest index modulations arise from birefringence produced by the dynamic orientation of the chromophores, a T_g close to room temperature is a desired property. Small molecules are often added to the mixture to act as plasticizers thereby lowering T_g.

Incredible advances have been accomplished in photorefractive polymer composites since their first discovery. A variety of different types of functional materials have been developed with large gain and high efficiency, such

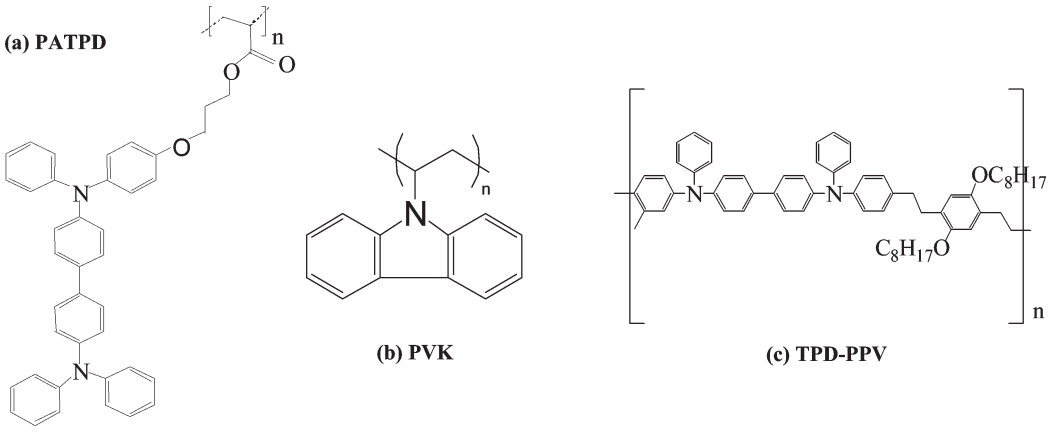

Figure 3. Some commonly used hole transporting polymers. (a) Tetraphenyldiaminobiphenyl (TPD) pendant group attached to a polyacrylate backbone through an alkoxy linker. (b) Poly(n-vinyl carbazole) (PVK). (c) Poly(arylene vinylene) copolymer (TPD-PPV).

as guest−host composites, fully functionalized polymers, polymer-dispersed liquid crystals, and amorphous glasses. This review will focus on guest−host composites, but reports on the properties of other types of PR materials are also available.[3,11] Guest−host composites delegate the functions required for photorefractivity to separate polymer constituents, allowing a high degree of customizability and wide range of material parameters to be achieved. This versatility generally comes at the cost of potential phase separation due to the mixing of polar and nonpolar molecules. Hence, careful material manipulations should be undertaken to achieve high quality photorefractive polymer composites.

Charge Transporting Agent (CTA). The CTA is an oxidizable host polymer that can efficiently transport charges leading to charge separation and the nonlocal nature of the PR effect. In the vast majority of samples, the holes are the most mobile carriers, though electron transport and trapping has also been studied and is discussed below.

Hereafter, all HOMO energy levels will be discussed with reference to that of the CTA. For the most commonly used CTAs, the HOMO is typically between −5.5 and −6.0 eV (referenced to vacuum level). A component with a HOMO energy level higher than that of the CTA means that its ionization potential is lower and a HOMO energy level lower than that of CTA means that its ionization potential is higher. To be effective, the CTA should be chosen such that the charge transporting moieties are highly conjugated with delocalized π-electrons. It should also be an electron donor capable of accepting a hole from the sensitizer molecule (in the case of hole transport). The latter condition requires that the sensitizer HOMO energy level be lower than that of the CTA to energetically facilitate charge transfer. Transport through the CTA will occur as electrons are transferred between charged and neutral moieties. The CTA is generally included with a high enough loading for transport to occur via hopping.[28] Large electric fields are applied because the mobility is highly field dependent.[29]

The chemical structures of some common CTAs are shown in Figure 3. Carbazole-containing polymers are very common and highly successful, such as poly(vinyl carbazole) (PVK), which the first high performance composites utilized,[2] and polysiloxane-based (PSX)[30] polymers. A few other conjugate polymers have drawn attention as well, because of the generally higher drift mobilities and reduced polarity leading to more stable mixing. Triarylamine-containing side chain polymers, such as poly(acrylic tetraphenyldiaminobiphenyl) (PATPD), have been as successful as PVK-based samples, and the response time is not dependent on the history of illumination,[31] as discussed below. Others include poly(phenylene vinylene) (PPV) copolymers, which have also shown superior steady-state performance compared to PVK systems.[32,33]

Nonlinear Chromophores. The chromophore provides the modulation of the refractive index in response to the development of the space-charge field. It can in general achieve this either through orientational birefringence or the linear electro-optic effect (or Pockels effect). Thus, the molecule must have either a large linear polarizability anisotropy (birefringence) or first hyperpolarizability (electro-optic), and in both cases must have a large ground state dipole moment. A widely accepted expression for quantifying the chromophore quality and optimizing these two contributions to the index modulation is[34]

$$\mathrm{FOM} = \frac{1}{M_W}\left[9\mu\beta + 2\frac{\mu^2\Delta\alpha}{k_B T}\right] \tag{4}$$

where M_W is the molar mass of the chromophore, μ is the dipole moment, β is the second-order polarizability, $\Delta\alpha$ is the linear polarizability anisotropy, k_B is Boltzmann's constant, and T is the temperature. A two-state four-orbital model assuming noninteracting electrons predicts that the hyperpolarizability maximizes for specific donor and acceptor strengths for the given conjugated bridge.[35] These predictions agree well with the experimentally observed values for β deduced from electric field-induced second harmonic generation measurements (EFISH), which measures the projection of the second-order polarizability tensor along the direction of the molecular dipole moment. A bond order alternation model has been proposed as a guide for optimizing the projection by adjusting the strengths of the acceptor and donor, and the

conjugated bridge length.[36] For the typical chromophores used in PR polymer composites, the contribution from the linear polarizability anisotropy is 1 order of magnitude higher than that from the first hyperpolarizability.[34] This is the molecular manifestation of the orientational enhancement, and states that the orientational birefringence is largely responsible for the performance. Note that this expression for the FOM arises from the oriented gas model,[37] which predicts the macroscopic properties of the material from the orientational distribution, density of molecules, and microscopic nonlinear properties. However, intermolecular interactions can occur, which are not accounted for in the model and can affect the performance, such as the interaction between the polar chromophore and the transport manifold, as discussed below.

Optimizing the dipole moment is an important step, as it can affect not just the modulation, but also, for example, the molecular aggregation, charge transport, and trapping. To achieve a permanent dipole moment, strong donor−acceptor termination groups are used to create electron separation across the π-conjugate bridge. Delocalization along a π-conjugated bridge permits rapid electronic redistribution in the presence of an electric field and will lead to noncentrosymmetry as a necessary condition for second-order nonlinear effects. This type of molecule is referred to as a push−pull molecule.[38] The dipole moment can also be tweeked by altering the length of the bridge, similar in principle to the quantum mechanical particle-in-a-box. However, longer bridge lengths may lead to reduced orientational freedom and increased optical absorption. Larger dipole moments will increase the FOM, but will also lead to phase instability of the composite as the highly polar chromophores begin to separate from other nonpolar molecules and crystallize out of the mixture. This also limits the chromophore density, which should be as large as possible for high modulation efficiency. In addition, highly polar chromophores with a large FOM will reduce the mobility of charges because of the energetic disorder introduced in the polymer matrix.[39]

The chromophores may also act as a sensitizer[10,19,40] if the energetics, absorption, and concentration is appropriate at the operational wavelength. For this to be effective, the HOMO level must be lower than that of the CTA to ensure charge injection (as with dicyanostyrenes and PATPD with a difference of about 0.4 eV) For the most commonly used CTAs, the HOMO is typically around −5.5 eV and the LUMO around −2.0 eV. If instead a chromophore with a HOMO level higher than that of the CTA is used, it may act as a (deep/shallow) trap[10,41] for holes already injected into the transport manifold from other sensitizers; the larger the gap, the more long-lived the trapping states will be. Typical PR chromophores have a HOMO level between −5 and −6 eV (referenced to vacuum level).

Thus, the ionization potential will affect the magnitude of the SC field and speed of the response.[42] The concentration is also an important parameter. If the HOMO level of chromophores is higher than that of the CTA, at low concentrations it will act as a trap. As the concentration increases the chromophore may also begin to participate in hole transport via hopping,[43] which will also lead to a trade off between a large SC field and fast response as the transport moiety is increased at the expense of trapping sites. In general, care must be taken to choose a chromophore with proper optical and electronic properties for the desired application, as this can affect not only the index modulation but also the charge generation, transport, and trapping.

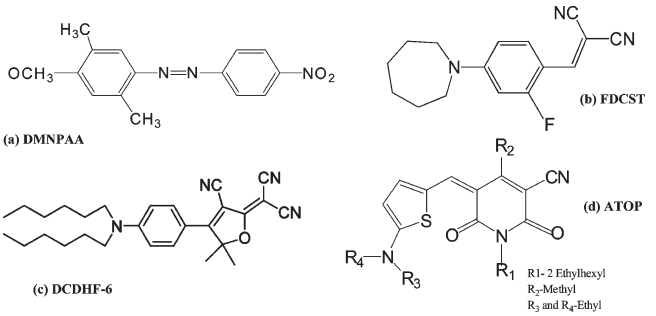

Figure 4. Some high-performing chromophores. (a) 2,5-Dimethyl-4-(p-phenylazo)anisole (DMNPAA). (b) Fluorinated dicyanostyrene 4-homopiperidino benzylidine malonitrile (FDCST). (c) 2-Dicyanomethylene-3-cyano-2,5-dihydrofuran (DCHHF-6). (d) Amino thienyl-dioxopyridine (ATOP).

A large number of chromophores have been developed for use in nonlinear optical applications. Among the most successful, are dicyanostyrenes (DCST),[44] azo-dye derivatives (DMNPAA),[45] and oxypriodine dyes (ATOP).[46] There have been recent trends toward tricyano molecules, such as DCDHF derivates, which have high photoconduction and TBC gain.[47,48] A number of reviews are available on the structure and design of chromophore for PR composites.[12,49,50] The structures for some of these chromophores are shown in Figure 4.

Sensitizer. Photogeneration of charges is provided by a molecule with sufficient proper absorption at the wavelength of interest. This is generally between 50 and 200 cm^{-1}; more transparent samples will not generate enough charges and more opaque samples can cause scattering, beam loss, and a reduction of the grating thickness. In certain cases, the sensitizer will form a charge transfer complex with the CTA, allowing the charges to be efficiently transferred between the separate functional components. In the case of primarily hole conduction, the sensitizer will inject a hole into the material by accepting an electron, becoming reduced. For the PR effect to be reversible, it should also be oxidizable to allow it to return to the original state. The sensitizer must also have the lowest HOMO and LUMO levels of all the components (typically −6 to 6.5 eV from vauum level). A lower HOMO ensures efficient charge injection to the CTA. Marcus' theory describes the physics of this charge-transfer process.[51] To obtain large photogeneration efficiency, the difference between the ionization potential of the donor and acceptor should be large.[52]

Sensitizer molecules may also act as traps after being reduced, as there is a correlation between the anion

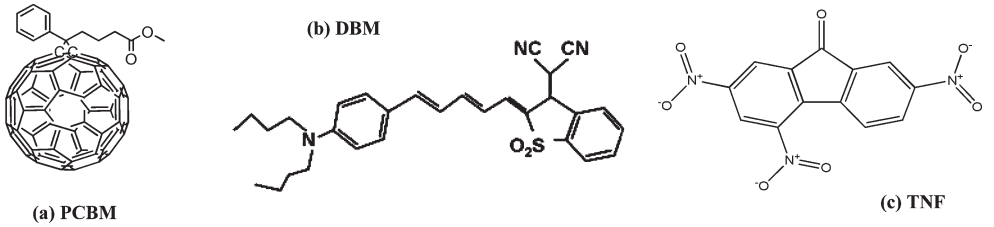

Figure 5. Typical sensitizer molecules. (a) [6,6]-Phenyl-C61-butyric acid-methylester (PCBM). (b) 2-[2-{5-[4-(Di-*n*-butylamino)phenyl]-2,4-pentadienylidene}-1,1-dioxido-1-benzothien-3(2H)-ylidene]malononitrile (DBM). (c) 2,4,7-Trinitro-9-fluorenone (TNF).

density and the trap density deduced from photorefractive performance characterization.[53] Moreover, the chromophore is involved in this process as well, as it can provide the compensating sites for the holes to balance the anion density. Without such sites, recombination would be more likely to occur. Thus, the ionization potential is similarly important in establishing the trap density.[54,55]

The most common and successful sensitizers are C_{60}, TNF, and TNFDM, (Figure 5) as they will form a strong CT complex with donor molecules. The highly soluble fullerene derivative, PCBM, is sometimes used in place of C_{60}, as similar solubility of the different constituents is a crucial prerequisite for guest−host polymers. These are mainly useful for spectral sensitivity in the visible region. DBM has also been used for sensitivity via two-photon absorption.[14] Other approaches have been studied, including inorganic nanocrystals such as CdSe and PbS,[56] which have the advantage of being tunable in their absorption band by changing the nanocrystal size. Despite the early discovery of the sensitization properties of C_{60} and the large number of studies that have succeeded this, it is still one of the best molecules for this purpose.

Plasticizer. Because the orientational birefringence is the largest source of index modulation, the T_g of the material must be at or near the operating temperature, which is normally room temperature. Usually the T_g of composites with high-molecular-weight polymers are much higher than room temperature. To counteract this, plasticizers may be added to the composite to reduce the T_g. They do not typically participate in charge generation and trapping, and are thus inert, though they do reduce the functional volume by diluting the charge transport matrix.

Benzyl butyl phthalate (BBP) is often used as a plasticizer in PVK-based composites, usually around a loading 15−20 wt %. A different approach is to make the plasticizer less inert by using the hole transporting monomeric carbazole unit as part of the design. The monomer, ethyl carbazole (ECZ), has shown excellent results with this approach as well in many composites,[57] though larger loadings may be needed to achieve a lower T_g than with BBP.

Recent Developments

Hole-Transporting Host Polymers. The first photorefractive polymer composites utilized diethylamino-benzaldehyde diphenylhydrazone (DEH) as the hole transporting molecule. The first high performance photorefractive polymers utilized PVK, which has since become one of the standards, with fast speed and high efficiency. However, a number of properties limit the usefulness of PVK in applications, such as a tendency of the components to aggregate and deterioration of the response time upon illumination.[53,54] Other polymers have been tried with some success, such as polysiloxane derivatives (PSX), which are similar to PVK in having a carbazole group, but in this case the backbone is a siloxane chain. PSX composites exhibit a lower T_g than PVK-based composites with similarly high performance,[58,59] and less tendency to phase separate.[60] Recently, a PVK polymer modified with 2-ethylhexanol was reported, which also reduces the T_g of the material compared to unmodified PVK.[61] A different class of the transporting polymers employ carbazole as a pendant group on a rigid backbone instead of a flexible one (as is typical), such as poly(*p*-phenylene terephthalate) (PPT).[62] These materials have a tendency to self-organize into layered microstructures, and have a glass transition below room temperature despite the lack of a plasticizer. They have demonstrated TBC gains over 200 cm^{-1} and diffraction efficiencies close to 100%. They even show improvements over PVK in reflection geometry where the small grating spacing often limits performance[63,64]

A different type of polymer is PATPD, which achieves hole transport without carbazole and the associated degradation of the stability and photorefractive properties.[31] This is due to the position of the HOMO level, which is above that of most chromophores. The energy levels of some typical constituents in PATPD and PVK composites are shown in Figure 6. With PVK, the mobile holes can be trapped in the chromophore HOMO, increasing the ionized acceptor density that is associated with deep trapping. With PATPD, it is not energetically favorable for the mobile holes to be injected into the chromophore HOMO. Thus, the ability of the chromophore to act as a compensating trap leading to the formation of C_{60} anions is reduced. The accumulation of traps degrades the photoconductivity and the response time of the grating as the material is exposed, and with PATPD this is avoided. Indeed, in PATPD composites, video-rate response times were maintained over a large range of exposures, whereas the response times of PVK-based composites deteriorated by about an order of magnitude, as shown in Figure 7. The composites studied were sensitized with C_{60} and contained either 7-DCST, DBDC, or a combination of the two as the chromophore. Response times were measured under 633 nm illumination with a total fluence of 1.1 W/cm^2.

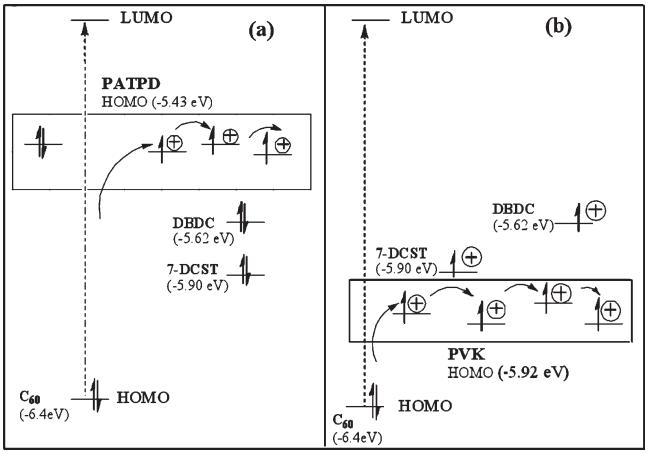

Figure 6. Comparison of trapping and transport sites of common components with (a) PATPD and (b) PVK. The more shallow HOMO level of PATPD reduces the density of deep traps. Reproduced with permission from ref 31. Copyright 2004 Wiley-VCH.

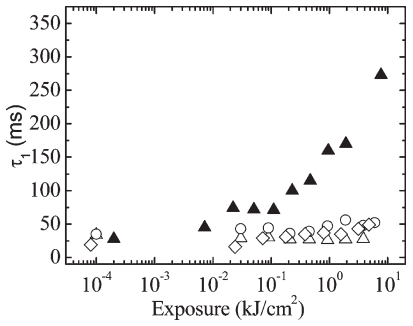

Figure 7. Dependence of fast time constant in transient FWM experiments on exposure. Open symbols are based on PATPD, filled triangles are based on PVK. Reproduced with permission from ref 31. Copyright 2004 Wiley-VCH.

The TPD is attached to a polyacrylic backbone through a flexible alkoxy linker, which reduces the T_g by providing structural flexibility and orientational freedom to the TPD. Thus, it is expected that the photorefractive traps are shallow, and conformational or structural in nature. Attempts have been made to modify the chromophore HOMO levels to mimic the situation in PVK materials, but this was achieved only at the expense of a dramatic reduction in the dynamic range.[54]

The phase stability of the composite was also enhanced, allowing chromophore loadings of 35−40%, and external diffraction efficiencies approaching 70% were achieved at fields of about 50 V/μm with net TBC gain coefficients well over 100 cm^{-1}. The hole mobility in TPD is also about 2 orders of magnitude higher than in PVK,[65] which may help increase the photogeneration efficiency; this high mobility is one of the reasons that TPD-based polymers have also found use in organic light-emitting diodes.[66,67]

Chromophores for High-Performance PR Composites. The design of nonlinear optical chromophores is also an active area, since this can affect nearly every functional property of the composites. There is no shortage of high performance composites. For example, PVK/DCDHF composites have exhibited TBC gains of 200 cm^{-1} with an absorption coefficient of 13 cm^{-1} at 647 nm and at only 30 V/μm.[47] PSX-based composites with the 2-piperidino-5-thienylmalononitrile (P-TH-DC) chromophore have recently shown near 100% diffraction efficiency at moderate fields of 50−70 V/μm and response times of about 100 ms.[59] At 532 nm, which is of interest for visual applications, PATPD and FDCST composites without C_{60} sensitization also have high diffraction efficiency.[19] In this case, the sensitization comes from the chromophore itself, and the ionization potential can be adjusted based on the position and degree of fluorination.[55] Liquid chromophores have also been used to achieve the PR effect without a plasticizer, demonstrating a response time of 46 ms.[68] Arylimine derivatives have exhibited near 100% diffraction efficiency and overmodulation at low fields (30−50 V/μm) with relatively low concentrations (25%),[69] though the gain coefficienct is well below 100 cm^{-1}.

Novel Methods of Increasing Sensitization. One persistent issue with organic PR polymers, particularly in the area of holographic recording, is the relatively low sensitivity compared to more traditional permanent emulsions. Thus, there are many ongoing efforts to improve sensitivity.

The most commonly used sensitizers thus far have been TNF, TNFM, and C_{60}, as well as the highly soluble counterpart to C_{60}, PCBM.[32] C_{60} was first reported in 1992,[70,71] as it was shown to be a good charge generator for PVK based composites. The first high gain and near 100% diffraction efficiency composites were based on TNF[2]. However, C_{60} has been shown to have an order of magnitude larger photogeneration efficiency than TNF in PVK-based composites,[72] as well as larger gain and faster PR response time.[47] TNF-C_{60} dyads have also been reported recently,[73] and exhibit a decrease in the grating response time as well as the beam fanning, which limits the fields that can be applied, compared to composites sensitized purely with C_{60}.

In addition to these standards, other techniques have been studied; in particular, inorganic quantum dots (QDs) have drawn much attention, primarily due to the ability to tune the spectral sensitivity across a wide range, from the visible to the IR. CdS and CdSe are typically used in the visible region and PbS and PbSe in the infrared. Quantum dots also have a photogeneration efficiency 1 order of magnitude larger than organically sensitized composites.[74] Other advantages are that a surface shell layer can be added, which has been shown to improve the index modulation and other performance parameters.[75] This is attributed to the suppression of mobile hole recombination because of the energy barrier provided by the large band gap surface layer.[76] Furthermore, the mobility of charges in the composites increases with QD concentration, despite the concentration remaining below the percolation threshold.[77] This has not been observed with organic sensitizers, and is due to the fact that with an applied electric field there is a potential difference of about 0.5 V across the semiconductor

quantum dots, but not so with organic molecules. The holes are more mobile inside the semiconductor nanoparticles than in the polymer matrix, and upon being absorbed, will be accelerated across the quantum dot by the potential difference.[78] It will therefore be reinjected with a higher velocity than when it entered. Thus, increasing the concentration will increase charge generation as well as the mobility.

Despite these advantages, QD composites have yet to achieve the same level of performance as all-organic polymers. The largest internal diffraction efficiencies are around 40% with NiS nanocrystals[79] (over 90% with CdS-sensitized polymer-dispersed liquid crystals[80]) and response times of about 100 ms or slightly less,[81] while many all-organic compositions exist with nearly 100% diffraction efficiency and video-rate response times. More in-depth review articles on nanoparticle-sensitized photorefractive polymers can be found in the literature.[82]

Some other unique approaches include using porphyrins like phthalocyanines (Pc), which have large absorptions in the visible, with energy level tuning achieved by changing the central atom. Recently, zinc and silicon Pc have been studied as the sensitizers in PVK-based composites.[83] For SiPc sensitized composites, the diffraction efficiency and response time are similar to PCBM composites, and the net gain coefficient is well above 200 cm^{-1} although higher concentrations are limited by the large absorption and scattering. The hole conducting polymer poly(3-hexylthiophene) (P3HT), often used in photovoltaics[84] and organic light-emitting diodes[85] was added in small concentrations to PSX-Cz composites to act as a sensitizer.[86] An order of magnitude increase in the PR grating speed was observed compared to C_{60} samples, albeit with an absorption coefficient of 181 cm^{-1}, versus 108 cm^{-1} for C_{60}. Use of a P3HT/C_{60} heterojunction as the sensitizer significantly decreased the absorption, as well as the speed of the grating formation, but did increase the magnitude of the steady-state SC field.

A significant spectral region where sensitivity is being improved is at IR and telecommunication wavelengths. This wavelength range is of importance not just for communication, but also for medical imaging, since this is where tissue is transparent. There are also available compact solid-state lasers operating at these wavelengths, making the implementation of such applications straightforward. A number of high performance composites have been demonstrated at 780 nm, with near 100% diffraction efficiencies.[42,87] This has been pushed to 830 nm with equally remarkable performance.[16,88−90] Three-dimensional imaging of living tissues using coherence-gated holography has been demonstrated at 835 nm using TPD and PCBM.[18]

Significant steps forward have been made to extend operation to even longer wavelengths with the use of other sensitizers. Single-walled carbon nanotubes have been used to sensitize at 1064 nm, though the diffraction efficiency is 1−2% with a speed of more than 1s in composites with aromatic polyimide.[91] Samples based on PVK exhibit a slightly decreased efficiency and two-beam coupling gain.[92] Composites with more standard sensitizers, such as DBM in a PATPD host matrix, have demonstrated 60% diffraction efficiency at 95 V/um and a response time of 33 ms at 975 nm[20]· PCBM and poly(*N*, *N*′-bis(4-hexylphenyl)-N′-(4-(9-phenyl-9H-fluoren-9-yl)-phenyl)-4,4′-benzidine) (PF6-TPD) samples achieve 76% diffraction efficiency at about 60 V/um and 36 ms response time at 1064 nm.[93] In the latter case, good performance is also achieved using the Ni-dithiolene complex TT-2324. The fast writing speeds in particular in these last two composites represent good progress toward realizing desired applications.

Even farther out, at 1340 and 1550 nm, novel sensitization schemes are required. Carbon nanotubes have been shown to operate in this region as well,[94] but with gain coefficients only around 30 cm^{-1}. PbS quatum dots have been used as a sensitizer at 1340 nm,[95] with very large net gain coefficients for quantum dot composites (over 100 cm^{-1}). PbSe has been used for 1550 nm, with 40% diffraction efficiency but with slightly reduced gain.[96] Both of these approaches suffer from slow grating buildup times (> 1 s) that are necessary for telecommuncations applications. Another material functioning at 1550 nm utilizes the organic dye DBM for sensitization via two-photon absorption.[14,23] This composite can achieve diffraction efficiency of 40% and with a video-rate response time of 33 ms. The two-photon absorption writing scheme also has the advantage of nondestructive read-out, but requires a high peak power pulsed laser.

A slightly variant to improving sensitivity comes not from new photosensitive functional components but by looking at the dynamics of electron transport and trapping. This phenomenon has been studied extensively with inorganic crystals,[97] and although holes are usually the dominant charge carrier in organic polymers, it is not without precedent for electrons to play an important role.[98,99] Explicitly electron-transporting materials have also been studied, with performance characteristics comparable to similar PVK-based materials, though not superior.[100]

The effect of electron traps has been studied in organic glasses with results that generally suggest faster grating buildup speeds and dynamics that depend on the concentration in more complicated ways than for unipolar materials.[101] You et al.[102] observed almost 2-fold increase in the net gain (to 235 cm^{-1}) with 0.05 wt % trapping molecules compared to a composite without traps. In fully functional polymers, tris(8-hydroxyquinoline) (Alq_3) electron traps were shown to reduce the grating response time one order of magnitude.[103] Similarly, in guest−host composites, Alq_3 has been shown to increase the gain, grating speed, and diffraction efficiency, as well as lead to bipolar transport.[104,105] The rational behind this approach is that electron traps can be added to reduce the probability of recombination with holes and improve the charge separation. The attractive advantage is that they can be added in small concentrations seemingly without affecting other aspects of the PR effect such as orientation. They also lead to increased dielectric breakdown

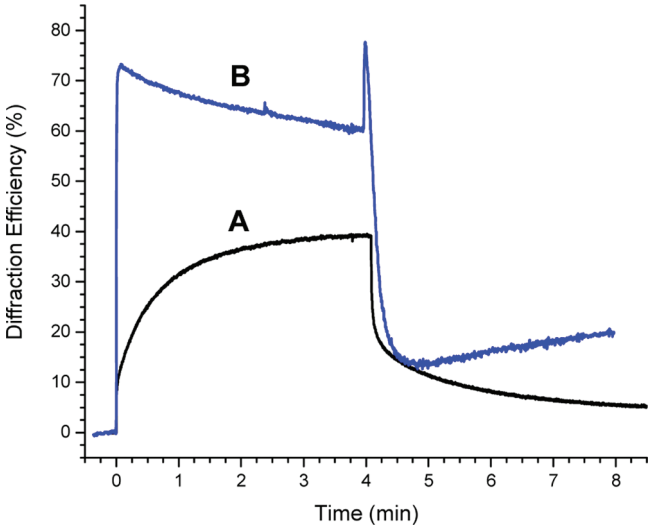

Figure 8. Transmission FWM response for (B) samples with 0.5 wt % of Alq_3 and (A) control samples without Alq_3. 532 nm writing beams are turned on at 0s and turned off at 4 min. (B) shows increased response time and recovery indicative of bipolar charge transport. Reproduced with permission from ref 105105. Copyright 2010 Optical Society.

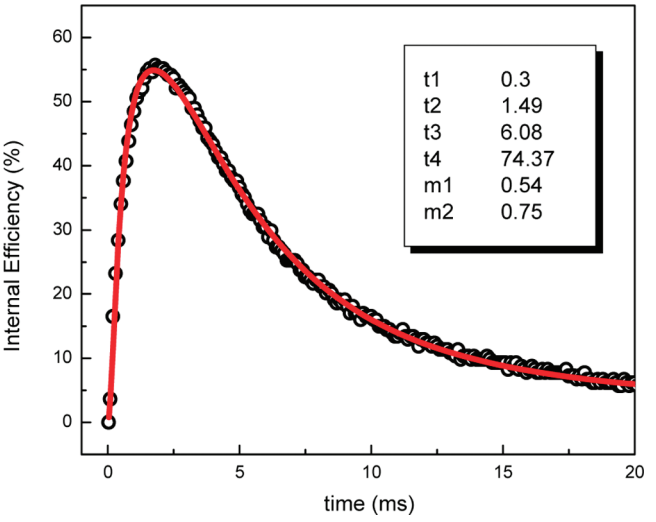

Figure 9. Simultaneous rise and decay of the diffraction efficiency under single pulse illumination. Pulse width was 1 ns and energy density was 4 mJ/cm^2, applied field was 95 V/μm. Reproduced with permission from ref 109. Copyright 2006 American Institute of Physics.

strength by suppressing electron transport but may contribute to phase instability.

In a recent recent report,[105] we have studied the effects on the FWM grating dynamics of adding 1 wt % Alq_3 to a composite with PATPD and 7-DCST (Figure 8). In this study, 532 nm writing beams with a total fluence of 200 mW/cm^2 were incident on the samples for about 4 min. The control samples reached a steady-state efficiency of about 40%, while the samples with Alq_3 achieved more than 70% in a much shorter time span. Moreover, the recovery of the efficiency after a short decay is indicative of bipolar charge transport, implying that apart from just reducing the recombination, the trapping effect from Alq_3 is also leading to a competing grating with opposite sign.

PR Polymer Composites for Applications

There are many proposed applications for organic PR polymers, for which all the previous material developments will assist to various degrees. They include tissue imaging,[18] beam cleanup,[106] data storage,[107] and dynamic displays.[19,108] In this section, we will review the specific material aspects required to realize some of these applications, namely pulsed writing required for many high speed devices, and holographic displays.

Pulsed Writing. One of the primary advantages of recording a grating with pulsed writing beams is that sufficient writing energy can be delivered in much shorter amounts of time than in CW. This will decrease the writing time but also makes the entire process very insensitive to vibration which can provide even further improvements in speed. The issue of decreasing overall writing time then transfers from delivering enough energy in a given time, to developing lasers with higher repetition rates. This requires a material that can respond to such brief impulses.

In one of our previous studies,[109] a PR composite consisting of PATPD/7-DCST/ECZ/C_{60} (54.5/25/20/0.5 wt %), 105 μm thick, was illuminated with two 532 nm writing beams about 1 ns in duration (total fluence of 4 mJ/cm^2). Under single pulse exposure, a maximum diffraction efficiency of 56% was observed in 1.8 ms after illumination, as charge transport, trapping, and chromophore orientation continued after illumination. An applied field of 95 V/μm was used in a standard geometry with a 60° slant and an interbeam angle of 20°. In CW recording, the same sample exhibits near 100% efficiency with a response time of 4 ms under a similar fluence.

Quantitative temporal characteristics were obtained by fitting the curve to a modified exponential function. Since grating formation and decay are occurring at the same time, each of which is typically characterized by two time constants, a total of four time constants were used:

$$\Delta n \propto [1 - m_1\exp(-t/t_1) - (1 - m_1)\exp(-t/t_2)] \times [m_2\exp(-t/t_3) + (1 - m_2)\exp(-t/t_4)] \quad (5)$$

$$\eta \propto \sin^2(B\Delta n)$$

All the fit parameters for single pulse illumination are shown in Figure 9. The fast time constant was 300 μs, with a weighting factor of 0.54. The slowest time constant for the decay portion was 74.4 ms.

The effect of pulse energy was studied by writing with different fluences. The fact that the peak power is also changing will not affect the PR process, since the number of charges generated is only affected by the total number of photons absorbed. The results of various pulse energies from 0.2 to 3 mJ/cm^2 are shown in Figure 10. The maximum efficiency increases approximately linearly with the energy, at least for the range used. However, the recording time does not significantly improve, suggesting the dynamics are not limited on these time scales

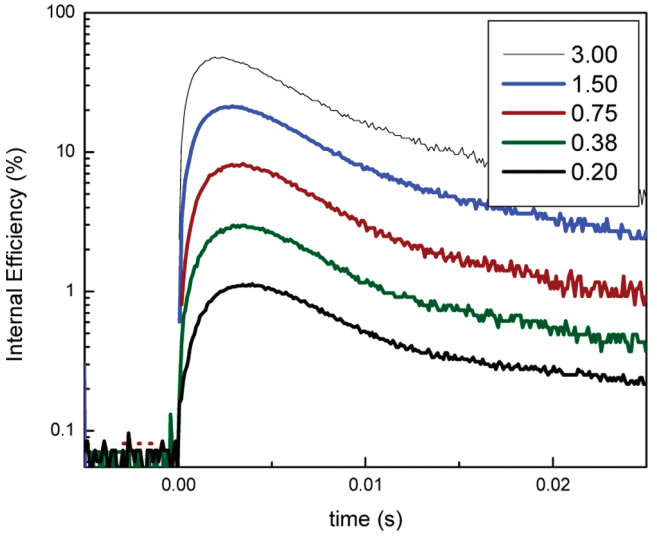

Figure 10. Response curve of diffraction efficiency under single pulse exposure with energy densities varying from 0.20 to 3.00 mJ/cm^2, as shown in the legend. Reproduced with permission from ref 109. Copyright 2006 American Institute of Physics.

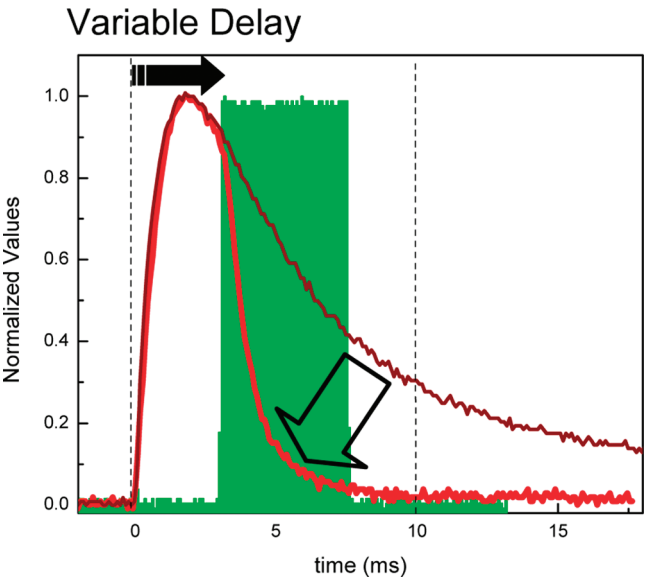

Figure 11. Response curve of diffraction efficiency with and without a separate uniform illumination to accelerate the decay. The green bar shows the duration of the cw erasing beam, with an energy of 6 mJ/cm^2. The grating has completely decayed in 10 ms, showing the potential for operation at 100 Hz. Reproduced with permission from ref 109. Copyright 2006 American Institute of Physics.

by charge generation but by the transport and orientation, which are independent of writing intensity. The dynamical processes under pulsed writing are different than with CW writing, because charges will be generated during the short exposure but all other processes related to grating formation will continue in the dark. The pulse does not persist long enough to reach steady-state and the magnitude of the SC field will depend on number of the charges generated. Thus, the diffraction efficiency is dependent on the writing intensity for the range of values used here. It is expected that for higher intensities the diffraction efficiency will saturate at the steady-state value obtained in CW at this voltage, though the energy needed may be much higher than is needed for CW.

A primary goal of such a device is to operate at the fastest possible speed for the desired application, at least as fast as the repetition rate, which can be around hundreds of hertz. To achieve this goal, the grating must form to a significant extent and decay within 10 ms so that new information can be recorded. The grating forms within 1−2 ms, and the decay can be accelerated by uniform illumination. Gated illumination for 5 ms with a CW 532 nm beam was used. The dynamics of this process are shown in Figure 11. Because it cannot be present during the grating formation, a variable time delay is used for the gating. At an energy density of 6 mJ/cm^2, the entire write-read-erase process was completed within 10 ms. The delay as well as the intensity and nature (cw or pulsed) of the erasing can be adjusted to optimize the signal-to-noise ratio during the reading process.

Although this constitutes a significant increase in the dynamic response, some applications will require even faster writing times, such as those involving large area devices and storage. A recent report,[107] shows a grating written with 130 fs pulses at 800 nm in PVK samples sensitized with TNFM. With an average intensity of 3.5 mW/cm^2, the diffraction efficiency reported is 2%, lower than for the PATPD samples under ns exposure, but much higher repetition rates are achievable (80 MHz) with these lasers; this would require materials with response times on the order of 10 ns. However, as faster lasers are used, the spectral bandwidth increases, which may reduce contrast from unintentional spectral multiplexing.

Updatable 3D Holographic Displays. Three-dimensional perception is fundamental to the human interaction with the world, because our brains are accustomed to processing more than just a single image to understand a situation. There are many applications where 3D displays would yield a significant advantage in terms of adaptation and functionality, including medical imaging, industrial design, and terrain mapping.

Current popular 3D imaging techniques rely on stereoscopic rendering that requires special eye-wear, at the expense of user fatigue and lack of depth. Holographic displays can reproduce very high quality images without these drawbacks, but to date have been made with either static photopolymers[110] or dynamic media with small-size and low resolution.[111,112]

Organic PR polymers have the potential to bridge this gap between speed and viewing experience, with large diffraction efficiencies, fast writing times, large area, phase stability, and reversible recording process. In 2008, such a composite has been demonstrated, combining all of these properties[19] into the first updatable holographic 3D display based on PR polymers. Recently, the composite was modified to improve the response under pulsed illumination and increase the recording speed to quasi-real-time and open up applications for 3D telepresence.[113] A copolymer is used as the hole-transporting agent to reduce the phase separation, allowing increased loading of the chromophores. The copolymer consists of a polyacrylic

backbone with pendant groups tetraphenyldiaminobiphenyl-type (TPD) and carbaldehyde aniline (CAAN) attached through an alkoxy linker (PATPD-CAAN) in a ratio of 10:1. A fluorinated dicyanostyrene (FDCST) NLO chromophore was added to provide sufficient refractive index change and charge generation at the wavelength of interest (532 nm). ECZ was also used to reduce the glass-transition temperature to room temperature. The ratios of PATPD:CAAN/FDCST/ECZ were 50/30/20 wt%. For pulsed illumination, 0.5 wt % of PCBM was added to increase the number of photogenerated charges. The display film was 105 μm thick with an active area of 4inches $\times$4inches for the display. It showed no phase separation in an accelerated aging test at 60 °C for 7 days, nor any degradation or damage for several months over hundreds of write/erase cycles. The absorption coefficient at 532 nm is 90 cm^{-1}.

This sample shows approximately 90% diffraction efficiency at 4 kV in the standard slanted transmission geometry at 532 nm CW illumination, as shown in Figure 12.

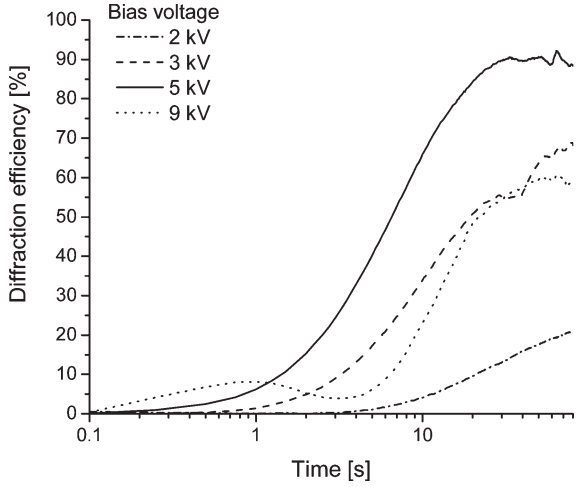

Figure 12. Dynamic response of the display sample from FWM at 532 nm under different applied voltages. While the largest efficiency is observed at 5 kV, near the overmodulation peak, the smallest time occurs at 9 kV, which is relevant for writing a holographic display. Reproduced with permission from ref 108. Copyright 2008 IEEE.

The transients in this geometry are shown in Figure 12 for various applied fields in the same geometry. Note that this sample is slower than the fast PR composites, though at 9 kV an intermediate peak is reached after 1s of writing. This permits writing the display at this voltage and sets the time scale of the recording process. Even though this peak is only at 10%, it is not the steady-state diffraction efficiency. This property is utilized in a voltage kick-off technique to provide high speed writing and long persistency. More details on the transients and writing techniques can be found elsewhere.[108]

The hologram for the 3D display is generated using integral image holography. More details on the writing system, including the optical setup, recording parameters, and hogel generation are discussed in the previous literature.[19] Briefly, dozens of 2D perspectives of an object are processed on a computer and then optically multiplexed onto the recording medium in a manner such that when reconstructed, the sensation of depth is created via parallax. The reference and object beam interfere in the sample in a Fourier transform geometry. The hologram is written by successively recording approximately 120 holographic pixels, or "hogels" side by side. In CW, given the geometry of the human vision, horizontal parallax only is used, so the hogels are vertical stripes. 532 nm light is used with a total writing intensity of 0.1 W/cm^2. Given the transients, each hogel is written for 1s, so the overall writing time is then 3−4 min for a 4 in. $\times$4 in. sample. After writing, the sample is translated to a new position and the hologram read using a 650 nm LED lamp. The image is visible for about 3 h of continuous viewing, but erasing can be done at any time by illuminating the sample with a homogeneous beam at 532 nm. In pulsed, the principle is similar; each hogel is written with a single 6 ns pulse from a 200 mJ laser with a repetition rate of 50 Hz. This decreases the writing time for a 4 inch sample to approximately 2 s, or by two orders of magnitude, to quasi-real-time. The total writing intensity was the same order of magnitude as used in the pulsed FWM experiments discussed above (10 mJ/cm^2). In this setup, the opto-mechanics move instead of the sample, which increases the overall time available to view the

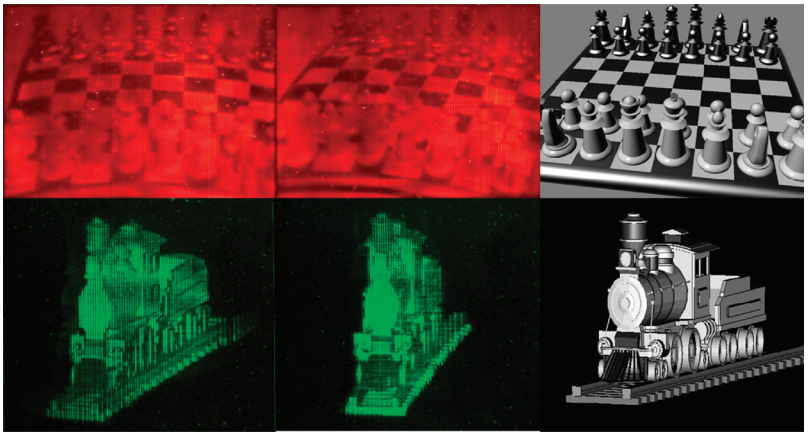

Figure 13. 2D images of the 3D holographic images produced from updatable display setup. Images are taken at different camera locations to demonstrate occlusion and parallax. The right-most images are one frame from the computer model used to generate the holograms. The top row is written with CW illumination, while the bottom row is written with pulsed.

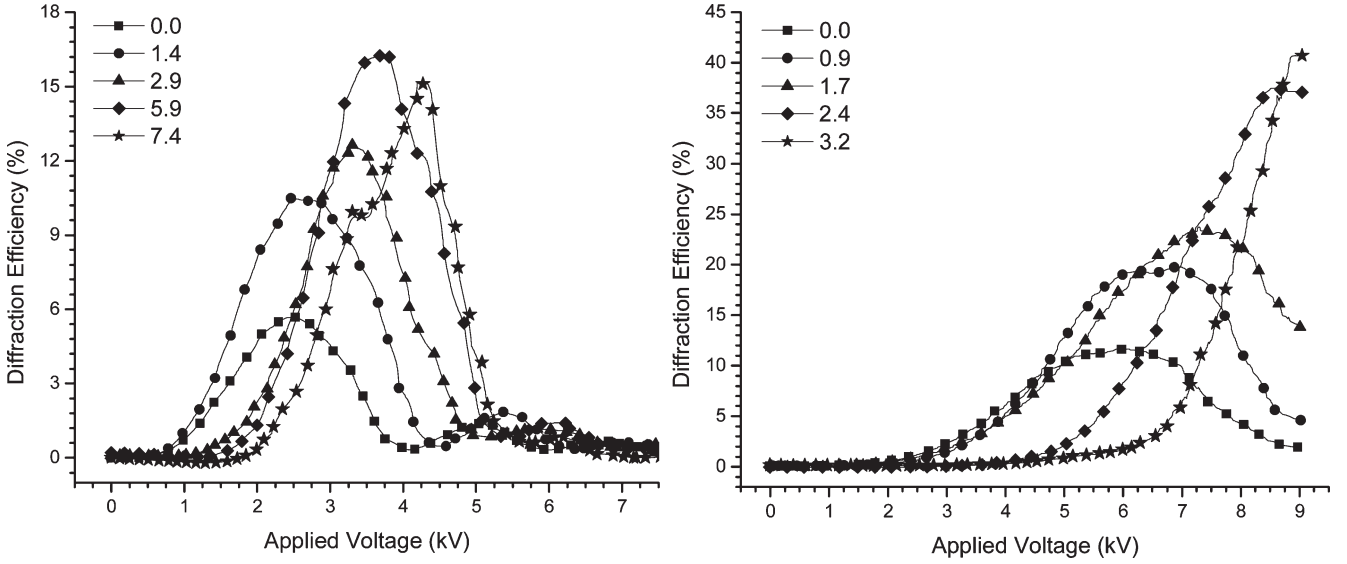

Figure 14. Steady-state diffraction efficiency in reflection of the display sample (left) and the same sample with 0.5 wt % of PCBM added (right). The numbers indicate the degrees offset of the reading beam from counter-propagation. The efficiency of the PCBM sample increases by more than a factor of 2. Reproduced with permission from ref 114. Copyright 2010 IEEE.

hologram before a successive image is written. The persistency of the image is also much shorter than in CW (5−60 s), due to the presence of PCBM and the writing technique, as is desired for 3D telepresence applications. Some images produced by these two writing processes are shown in Figure 13.

Although this constitutes significant progress in the area of holographic displays, many applications will require faster samples for use in video-rate displays, and practicality dictates the viewability in standard white light room conditions. This latter requirement is accomplished in reflection geometry, and the results from FWM experiments are shown in Figure 14 (left). In this measurement, the writing beams still have an interbeam angle of 36°, but the plane of the sample is along the bisector. The peak efficiency exhibited was 16% at 3.6 kV. However, an offset from counter-propagating for the reading beam is needed to achieve even this level of efficiency. This is because as the field is increased, the chromophores align with both the sinusoidally varying SC field as well as the DC applied field. Thus, the refractive index modulation has both an AC and DC component. The DC change will alter the refracted angle of the reading beam, requiring an angle different from counter-propagation to be Bragg-matched. So instead of following a $\tanh^2(B\Delta n)$, the efficiency starts to drop as the field increases and reduces the Bragg matching.[114] This is an issue in reflection as opposed to transmission since reflection gratings are much more selective. For this particular sample, a 6° shift is required to restore Bragg-matching.

In this writing configuration, the grating spacing is 0.2 μm, which is a factor of 6.5 smaller than in transmission. To accurately reproduce this interference pattern, higher trap densities are needed. To this end, PCBM was added at 0.5 wt % to the previously mentioned display composition both as a charge generator and a charge trap.[115] It is also expected that this approach will be necessary to improve the speed of sample for use in video-rate displays, as discussed above. Apart from this, the design and fabrication of this sample is identical to the previous one. The results of FWM in reflection for this sample are also included in Figure 14 (right); we observe 40% diffraction efficiency at 9 kV and an offset of 3°. The increased trap density leads directly to a larger SC field, but likely also reduces the recombination, both of which explain the increase in efficiency.

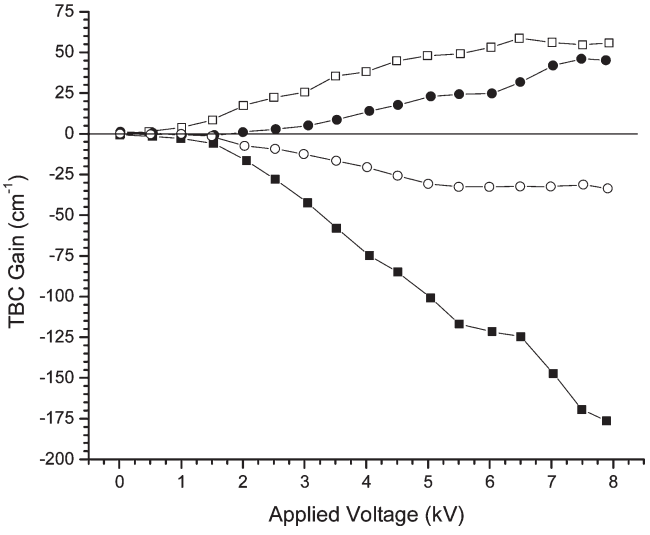

Figure 15. Two-beam coupling gain at 532 nm in transmission (solid) and reflection (open) of samples without (squares) and with (circles) PCBM. The reversal of the sign in reflection is consistent with a birefringence dominated effect. The reversal of the sign with PCBM is evidence of a change in the sign of the majority charge carrier. Reproduced with permission from ref 114. Copyright 2010 IEEE.

The addition of PCBM has other anticipated changes, as evidenced by the TBC data in Figure 15. These measurements are performed in the same geometry (negative electrode facing the incident beams to reduce fanning) with the same parameters as the FWM measurements,

except the writing beams were p-polarized. The sign of the gain reverses in going from transmission to reflection, consistent with a PR effect dominated by orientational birefringence. In both geometries, the addition of PCBM reverses the sign of the gain, which suggests one sample is hole-dominated and one is electron-dominated. It is likely the PCBM is the hole-dominated sample, because it acts as hole trap under illumination and the direction is the same as other hole-dominated samples. The presence of competing gratings in these samples makes the optimization of trap densities and functional components more complicated, though as discussed above, bipolar materials have shown excellent properties.

Summary and Outlook

Photorefractive polymers have advanced to such a level that devices with large figures-of-merit are readily available. They outperform their inorganic counterparts in diffraction efficiency, sensitivity and two beam coupling gain. They are attractive for the reversibility of the process, sensitivity from the visible to the infrared, and highly customizable fabrication, so that new ideas can be tried with relative ease. Thus, the current forefront of the research is on developing materials for specific applications and assessing their performance in real-world schemes. In particular, recent applications that have been demonstrated include 3D holographic displays with potential medical, military, and industry uses, and accurate imaging through highly scattering media such as tissue for noninvasive diagnoses.

Recent material advancements that have made these possible include the development of hole-transporting polymers with large mobilities, low T_g, excellent phase stability, and stable dynamics, such as PATPD. Extensions of the sensitivity using nonstandard materials such as inorganic nanocrystals result in charge generation rates larger than the long-used C_{60} composites. Using low ionization potential molecules, the spectral sensitivity has also been extended to the near-IR and even telecommunications wavelengths using TPA.

Despite the rapid progress, there is still much left to be accomplished. The sensitivity in particular is much less than photographic films at least for holographic applications, though the updatability is a significant advantage. Many of the complex processes are still only vaguely understood, and modeling efforts will need to be stepped up to better understand the physics and guide developments. In addition, the electrical and chemical stability is still an issue for some composites. The emerging applications will continue to drive the scientific community in the development of new materials to meet these challenges.

Acknowledgment. The authors acknowledge support from AFOSR, DARPA, and NSF ERC Center on Integrated Access Networks (CIAN).

References

(1) Ducharme, S.; Scott, J. C; Moerner, W. E. *Phys. Rev. Lett.* **1991**, *66*, 1846.
(2) Meerholz, K.; Volodin, B. L.; Sandalphon; Kippelen, B.; Peyghambarian, N. *Nature* **1994**, *371*, 497.
(3) Ostroverkhova, O.; Moerner, W. E. *Chem. Rev.* **2004**, *104*, 3267.
(4) Thomas, J.; Norwood, R. A.; Peyghambarian, N. In *New Directions in Holography and Speckle*; Caulfield, H. J., Vikram, C. S., Eds.; American Scientific Publishers: Valencia, CA, 2008.
(5) Ashkin, A.; Boyd, G. D.; Dziedzic, J. M.; Smith, R. G.; Ballman, A. A.; Levinste, J. J.; Nassau, K. *Appl. Phys. Lett.* **1966**, *9*, 72.
(6) Chen, F. S. *J. Appl. Phys.* **1967**, *38*, 3418.
(7) Staebler, D. L. *Appl. Phys. Lett.* **1975**, *26*, 182.
(8) Staebler, D. L.; Amodei, J. J. *J. Appl. Phys.* **1972**, *43*, 1042.
(9) Schildkraut, J. S.; Cui, Y. *J. Appl. Phys.* **1992**, *72*, 5055.
(10) Ostroverkhova, O.; Singer, K. D. *J. Appl. Phys.* **2002**, *92*, 1727.
(11) Moerner, W. E.; Grunnet-Jepsen, A.; Thompson, C. L. *Annu. Rev. Mater. Sci.* **1997**, *27*, 585.
(12) Marder, S. R.; Kippelen, B.; Jen, A. K.-Y.; Peyghambarian, N. *Nature* **1997**, *388*, 845.
(13) Günter, P.; Huignard, J.-P. *Photorefractive Materials and Their Applications I, II and III*; Springer-Verlag: Berlin, 1988.
(14) Tay, S.; Thomas, J.; Eralp, M.; Li, G.; Kippelen, B.; Marder, S. R.; Meredith, G.; Schülzgen, A.; Peyghambarian, N. *Appl. Phys. Lett.* **2004**, *85*, 4561.
(15) Volodin, B. L.; Kippelen, B.; Meerholz, K.; Peyghambarian, N.; Javidi, B. A. *Nature* **1996**, *383*, 58.
(16) Kippelen, B.; Marder, S. R.; Hendrickx, E.; Maldonado, J. L.; Guillemet, G.; Volodin, B. L.; Steele, D. D.; Enami, Y.; Sandalphon; Yao, Y. J.; Wang, J. F.; Röckel, H.; Erskine, L.; Peyghambarian, N. *Science* **1998**, *279*, 54.
(17) Winiarz, J. G.; Ghebremichael, F.; Thomas, J.; Meredith, G.; Peyghambarian, N. *Opt. Express* **2004**, *12*, 2517.
(18) Salvador, M.; Prauzner, J.; Köber, S.; Meerholz, K.; Turek, J. J.; Jeong, K.; Nolte, D. D. *Opt. Express* **2009**, *14*, 11834.
(19) Tay, S.; Blanche, P.-A.; Voorakaranam, R.; Tunç, A. V.; Lin, W.; Rokutanda, S.; Gu, T.; Flores, D.; Wang, P.; Li, G.; Hilaire, P., St.; Thomas, J.; Norwood, R. A.; Yamamoto, M.; Peyghambarian, N. *Nature* **2007**, *451*, 694.
(20) Eralp, M.; Thomas, J.; Tay, S.; Li, G.; Meredith, G.; Schulzgen, A.; Peyghambarian, N.; Walker, G. A.; Barlow, S.; Marder, S. R. *Appl. Phys. Lett.* **2004**, *85*, 1095.
(21) Köber, S.; Prauzner, J.; Salvador, M.; Kooistra, F.; Hummelen, J.; Meerholz, K. *Adv. Mater.* **2010**, *22*, 1383.
(22) Choudhury, K. R.; Sahoo, Y.; Jang, S. J.; Prasad, P. N. *Adv. Funct. Mater.* **2005**, *15*, 751.
(23) Tay, S.; Thomas, J.; Eralp, M.; Li, G.; Norwood, R. A.; Schülzgen, A.; Yamamoto, M.; Barlow, S.; Walker, G. A.; Marder, S. R.; Peyghambarian, N. *Appl. Phys. Lett.* **2005**, *87*, 171105.
(24) Blanche, P.-A.; Kippelen, B.; Schulzgen, A.; Fuentes-Hernandez, C.; Ramos-Ortiz, G.; Wang, J. F.; Hendrickx, E.; Peyghambarian, N.; Marder, S. R. *Opt. Lett.* **2002**, *27*, 19.
(25) Kippelen, B. Organic Photorefractive Materials and Their Applications. In *Photorefractive Materials and Their Applications 2*; Günter, P, Huignard, J.-P., Eds.; Springer: Berlin, 2007.
(26) Moerner, W. E.; Silence, S. M.; Hache, F.; Bjorklund, G. C. *J. Opt. Soc. Am. B* **1994**, *11*, 320.
(27) Cheng, N.; Swedek Prasad, P. N. *Appl. Phys. Lett.* **1997**, *71*, 1828.
(28) Bässler, H. *Phys. Status Solidi B* **1993**, *175*, 15.
(29) Pautmeier, L.; Richert, R.; Bässler, H. *Synth. Met.* **1990**, *37*, 271.
(30) Zhang, Y.; Wada, T.; Sasabe, H. *J. Mater. Chem.* **1998**, *8*, 809.
(31) Thomas, J.; Fuentes-Hernandez, C.; Yamamoto, M.; Cammack, K; Matsumoto, K.; Walker, G. A.; Barlow, S.; Kippelen, B.; Meredith, G.; Marder, S. R.; Peyghambarian, N. *Adv. Mater.* **2004**, *16*, 2032.
(32) Mecher, E. H.; Brauchle, C.; Horhold, H. H.; Hummelen, J. C.; Meerholz, K. *Phys. Chem. Chem. Phys.* **1999**, *1*, 1749.
(33) Horhold, H. H.; Tillmann, H.; Raabe, D.; Helbig, M.; Elflein, W.; Brauer, A.; Holzer, W.; Penzkofer, A. *Proc. SPIE* **2001**, *4105*, 431.
(34) Wortmann, R.; Poga, C.; Twieg, R. J.; Geletneky, C.; Moylan, C. R.; Lundquist, P. M.; DeVoe, R. G.; Cotts, P. M.; Horn, H.; Rice, J. E.; Burland, D. M. *J. Chem. Phys.* **1996**, *105*, 10637.
(35) Marder, S. R.; Beratan, D. N.; Cheng, L. T. *Science* **1991**, *252*, 103.
(36) Meyers, F.; Marder, S. R.; Pierce, B. M.; Bredas, J. L. *J. Am. Chem. Soc.* **1994**, *116*, 10703.
(37) Burland, D. M.; Miller, R. D.; Walsh, C. A. *Chem. Rev.* **1994**, *94*, 31.
(38) Kippelen, B.; Meerholz, K. Peyghambarian, N. An introduction to photorefractive polymers. In *Nonlinear Optics of Organic Molecules and Polymers*; Nalwa, H. S.; Miyata, S., Eds.; CRC Press, Boca Raton, FL, 1997.
(39) Goonesekera, A.; Ducharme, S. *J. Appl. Phys.* **1999**, *85*, 6506.
(40) Quintana, J. A.; Boj, P. G.; Villalvilla, J. M.; Ortiz, J.; Fernandez-Lazaro, F.; Sastre-Santos, A.; Diaz-Garcia, M. A. *Appl. Phys. Lett.* **2005**, *87*, 261111.
(41) Daubler, T. K.; Bittner, R.; Meerholz, K.; Cimrova, V.; Neher, D. *Phys. Rev. B* **2000**, *61*, 13515.
(42) Van Steenwinckel, D.; Hendrickx, E.; Persoons, A.; Van den Broeck, K.; Samyn, C. *J. Chem. Phys.* **2000**, *112*, 11030.
(43) Oh, J.; Lee, C.; Kim, N. *J. Appl. Phys.* **2008**, *104*, 073709.
(44) Wright, D.; Diaz-Garcia, M. A.; Casperson, J. D.; DeClue, M.; Moerner, W. E.; Twieg, R. J. *Appl. Phys. Lett.* **1998**, *73*, 1490.

(45) Bauml, G.; Schloter, S.; Hofmann, U.; Haarer, D. *Synth. Met*. **1998**, *97*, 165.
(46) Meerholz, K.; De Nardin, Y.; Bittner, R.; Wortmann, R.; Wurthner, F. *Appl. Phys. Lett*. **1998**, *73*, 4.
(47) Ostroverkhova, O.; Gubler, U.; Wright, D.; Moerner, W. E.; He, M.; Twieg, R. *Adv. Funct. Mat*. **2002**, *12*, 621.
(48) Hou, Z.; You, W.; Yu, L. P. *Appl. Phys. Lett*. **2003**, *82*, 3385.
(49) Wurthner, F.; Wortmann, R.; Meerholz, K. *ChemPhysChem* **2002**, *1*, 17.
(50) Bittner, R.; Meerholz, K. In *Photorefractive Materials and Their Applications III*; Günter, P., Huignard, J.-P., Eds.; Springer-Verlag: Berlin, 2007.
(51) Marcus, R. A. *Rev. Mod. Phys*. **1993**, *65*, 599.
(52) Hendrickx, E.; Van Steenwinckel, D.; Persoons, A.; Samyn, C.; Beljonne, D.; Bredas, J. L. *J. Chem. Phys*. **2000**, *113*, 5439.
(53) Grunnet-Jepsen, A.; Wright, D.; Smith, B.; Bratcher, M. S.; DeClue, M. S.; Siegel, J. S.; Moerner, W. E. *Chem. Phys. Lett*. **1998**, *291*, 553.
(54) Herlocker, J. A.; Fuentes-Hernandez, C.; Ferrio, K. B.; Hendrickx, E.; Blanche, P.-A.; Peyghambarian, N.; Kippelen, B.; Zhang, Y.; Wang, J. F.; Marder, S. R. *Appl. Phys. Lett*. **2000**, *77*, 2292.
(55) Hendrickx, E.; Zhang, Y. D.; Ferrio, K. B.; Herlocker, J. A.; Anderson, J.; Armstrong, N. R.; Mash, E. A.; Persoons, A. P.; Peyghambarian, N.; Kippelen, B. *J. Mater. Chem*. **1999**, *9*, 2251.
(56) Li, X.; Chon, J. W. M.; Gu, M. *Aust. J. Chem*. **2008**, *61*, 317.
(57) Van Steenwinckel, D.; Hendrickx, E.; Samyn, C.; Engels, C.; Persoons, A. *J. Mater. Chem*. **2000**, *10*, 2692.
(58) Zobel, O.; Eckl, M.; Strohriegl, P.; Haarer, D. *Adv. Mater*. **1995**, *7*, 911.
(59) Choi, C.; Nguyen, Q. V.; Kim, N. *Macromol. Res*. **2010**, *18*, 279.
(60) Moon, I. K.; Choi, C.; Kim, N. *Opt. Mater*. **2009**, *31*, 1017.
(61) Moon, I. K.; Choi, C.; Kim, N. *J. Polym. Sci., Polym. Phys*. **2009**, *47*, 1695.
(62) Kwon, O. P.; Lee, S. H.; Montemezzani, G.; Gunter, P. *Adv. Funct. Mater*. **2003**, *13*, 434.
(63) Kwon, O. P.; Montemezzani, G.; Gunter, P.; Lee, S. H. *Appl. Phys. Lett*. **2004**, *84*, 43.
(64) Kwon, O. P.; Kwon, S. J.; Jazbinsek, M.; Lee, S. H.; Gunter, P. *Polymer* **2005**, *46*, 10301.
(65) Ogino, K.; Nomura, T.; Shichi, T.; Park, S.-H.; Sato, H.; Aoyama, T.; Wada, T. *Chem. Mater*. **1997**, *9*, 2768.
(66) Miller, R. D.; Lee, V. Y.; Twieg, R. J. *Chem. Commun*. **1995**, 245.
(67) Yamamori, A.; Adachi, C.; Koyama, T.; Taniguchi, Y. J. *J. Appl. Phys*. **1999**, *86*, 4369.
(68) Choi, C.; Moon, I. K.; Kim, N. *Macromol. Res*. **2009**, *17*, 874.
(69) Maldonado, J. L.; Ponce-de-Leon, Y.; Ramos-Ortiz, G.; Rodriguez, M.; Meneses-Nava, M. A.; Barbosa-Garcia, O.; Santillan, R.; Farfan, N. *J. Phys. D*. **2009**, *42*, 075102.
(70) Zhang, Y.; Cui, Y. P.; Prasad, P. N. *Phys. Rev. B* **1992**, *46*, 9900.
(71) Silence, S. M.; Walsh, C. A.; Scott, J. C.; Matray, T. J.; Twieg, R. J.; Hache, F.; Bjorklund, G. C.; Moerner, W. E. *Opt. Lett*. **1992**, *17*, 1107.
(72) Hendrickx, E.; Zhang, Y. D.; Ferrio, K. B.; Herlocker, J. A.; Anderson, J.; Armstrong, N. R.; Mash, E. A.; Persoons, A. P.; Peyghambarian, N.; Kippelen, B. *J. Mater. Chem*. **1999**, *9*, 2251.
(73) Ortiz, J.; Fernandez-Lazaro, F.; Sastre-Santos, A.; Quintana, J. A.; Villalvilla, J. M.; Boj, P.; Diaz-Garcia, M. A.; Rivera, J. A.; Stepleton, S. E.; Cox, C. T.; Echegoyen, L. *Chem. Mater*. **2004**, *16*, 5021.
(74) Winiarz, J. G.; Zhang, L. M.; Lal, M.; Friend, C. S.; Prasad, P. N. *Chem. Phys*. **1999**, *245*, 417.
(75) Binks, D. J.; Bant, S. P.; West, D. P.; O'Brien, P.; Malik, M. A. *J. Mod. Opt*. **2003**, *50*, 299.
(76) Aslam, F.; Graham, D. M.; Binks, D. J.; Dawson, P.; Pickett, N.; O'Brien, P.; Byeon, C. C.; Ko, D.; Lee, J. *J. Appl. Phys*. **2008**, *103*, 093702.
(77) Choudhury, K. R.; Winiarz, J. G.; Samoc, M.; Prasad, P. N. *Appl. Phys. Lett*. **2003**, *82*, 406.
(78) Choudhury, K. R.; Samoc, M.; Patra, A.; Prasad, P. N. *J. Phys. Chem. B* **2004**, *108*, 1556.
(79) Fears, T. M.; Anderson, C.; Winiarz, J. G. *J. Chem. Phys*. **2008**, *129*, 154704.
(80) Winiarz, J. G.; Prasad, P. N. *Opt. Lett*. **2002**, *27*, 1330.
(81) Fuentes-Hernandez, C.; Suh, D. J.; Kippelen, B.; Marder, S. R. *Appl. Phys. Lett*. **2004**, *85*, 534.
(82) Li, X.; Chon, J. W. M.; Gu, M. *Aust. J. Chem*. **2008**, *61*, 317.
(83) Gallego-Gomez, F.; Quintana, J. A.; Villalvilla, J. M.; Diaz-Garcia, M. A.; Martin-Gomis, L.; Fernandez-Lazaro, F.; Sastre-Santos, A. *Chem. Mater*. **2009**, *21*, 2714.
(84) Brabec, C. J.; Dyakonov, V.; Parisi, J.; Sariciftci, N. S. *Organic Photovoltaics: Concepts and Realization*; Springer-Verlag: Berlin, 2003.
(85) Shinar, J. *Organic Light Emitting Devices: A Survey*; American Institute of Physics: New York, 2002.
(86) Oh, J.; Choi, J.; Luong, B. T.; Kim, N. *Macromol. Res*. **2010**, *18*, 8.
(87) Hendrickx, E.; Van Steenwinckel, D.; Persoons, A. *Appl. Opt*. **2001**, *9*, 1412.
(88) Mecher, E.; Gallego-Gomez, F.; Tillmann, H.; Horhold, H. H.; Hummelen, J. C.; Meerholz, K. *Nature* **2002**, *418*, 959.
(89) Ostroverkhova, O.; Moerner, W. E.; He, M.; Tweig, R. J. *Appl. Phys. Lett*. **2003**, *82*, 3602.
(90) Mecher, E.; Gallego-Gomez, F.; Meerholz, K.; Tillmann, H.; Horhold, H. H.; Hummelen, J. C. *ChemPhysChem* **2004**, *5*, 277.
(91) Vannikov, A. V.; Rychwalski, R. W.; Grishina, A. D.; Pereshivko, L. Y.; Krivenko, T. V.; Savel'ev, V. V.; Zolotarevskii, V. I. *Opt. Spectrosc*. **2005**, *99*, 643.
(92) Grishina, A. D.; Licea-Jimenez, L.; Pereshivko, L. Y.; Krivenko, T. V.; Savel'ev, V. V.; Rychwalski, R. W.; Vannikov, A. V. *High Energ. Chem*. **2006**, *40*, 341.
(93) Köber, S.; Prauzner, J.; Salvador, M.; Kooistra, F.; Hummelen, J.; Meerholz, K. *Adv. Mater*. **2010**, *22*, 1383.
(94) Grishina, A. D.; Pereshivko, L. Y.; Licea-Jimenez, L.; Krivenko, T. V.; Savel'ev, V. V.; Rychwalski, R. W.; Vannikov, A. V. *High Energy Chem*. **2007**, *41*, 267.
(95) Choudhury, K. R.; Sahoo, Y.; Jang, S. J.; Prasad, P. N. *Adv. Funct. Mater*. **2005**, *15*, 751.
(96) Choudhury, K. R.; Sahoo, Y.; Prasad, P. N. *Adv. Mater*. **2005**, *17*, 2877.
(97) Solymar, L.; Webb, D. J.; Grunnet-Jepsen, A. *The Physics and Applications of Photorefractive Materials*; Clarendon Press: Oxford, U.K., 1996.
(98) Wang, L. M.; Ng, M. K.; Yu, L. P. *Phys. Rev. B* **2000**, *62*, 4973.
(99) Salvador, M.; Gallego-Gomez, F.; Koeber, S.; Meerholz, K. *Appl. Phys. Lett*. **2007**, *90*, 154102.
(100) Okamoto, K.; Nomura, T.; Park, S. H.; Ogino, K.; Sato, H. *Chem. Mater*. **1999**, *11*, 3279.
(101) Sohn, J.; Hwang, J.; Park, S. Y.; Noh, Y. Y.; Kim, J. J. *Appl. Phys. Lett*. **2002**, *81*, 190.
(102) You, W.; Hou, Z. J.; Yu, L. P. *Adv. Mater*. **2004**, *16*, 356.
(103) Zhang, J.; Chen, Z. J.; Liu, Y. H.; Huang, M. M.; Wei, Q.; Gong, Q. H. *Appl. Phys. Lett*. **2004**, *85*, 1323.
(104) Wei, Q.; Liu, Y. H.; Chen, Z. J.; Huang, M. M.; Zhang, J.; Gong, Q,H.; Chen, X. F.; Zhou, Q. F. *J. Opt. A* **2004**, *6*, 890.
(105) Christenson, C. W.; Thomas, J.; Blanche, P.; Voorakaranam, R.; Norwood, R.; Yamamoto, M.; Peyghambarian, N. *Opt. Express* **2010**, *18*, 9358.
(106) Winiarz, J. G.; Ghebremichael, F.; Thomas, J.; Meredith, G.; Peyghambarian, N. *Opt. Express* **2004**, *12*, 2517.
(107) Nau, D.; Christ, A.; Giessen, H.; Wagner, A.; Euteneuer, A.; Salvador, M.; Mecher, E.; Meerholz, K. *Appl. Phys. B: Laser Opt*. **2009**, *95*, 31.
(108) Blanche, P.; Tay, S.; Voorakaranam, R.; Saint-Hilaire, P.; Christenson, C.; Gu, T.; Lin, W.; Flores, D.; Wang, P.; Yamamoto, M.; Thomas, J.; Norwood, R. A.; Peyghambarian, N. *J. Disp. Technol*. **2008**, *4*, 424.
(109) Eralp, M.; Thomas, J.; Tay, S.; Schulzgen, A.; Norwood, R. A.; Yamamoto, M.; Peyghambarian, N. *Appl. Phys. Lett*. **2006**, *89*, 114015.
(110) Zebra Imaging, Inc.; Klug, M. A.; Newswanger, C.; Huang, Q.; Holzbach, M. E. Active Digital Hologram Display; U.S. Patent 7 227 674, June 5, 2007.
(111) Hilaire, P. S.; Lucente, M. A.; Benton, S. A. *J. Opt. Soc. Am. A* **1992**, *9*, 1969.
(112) Huebschman, M. L.; Munjuluri, B.; Garner, H. R. *Opt. Express* **2003**, *11*, 437.
(113) Blanche, P.-A.; Bablumian, A.; Voorakaranam, R.; Christenson, C.; Lin, W.; Gu, T.; Flores, D.; Wang, P.; Hsieh, W.-Y.; Kathaperumal, M.; Rachwal, B.; Siddiqui, O.; Thomas, J.; Norwood, R. A.; Yamamoto, M.; Peyghambarian, N. *Nature* **2010**, *468*, 80.
(114) Eralp, M.; Thomas, J.; Tay, S.; Blanche, P.-A.; Schuelzgen, A.; Norwood, R. A.; Yamamoto, M.; Peyghambarian, N. *Opt. Express* **2007**, 11622.
(115) Christenson, C. W.; Blanche, P.-A.; Tay, S.; Voorakaranam, R.; Gu, T.; Lin, W.; Wang, P.; Yamamoto, M.; Thomas, J.; Norwood, R. A.; Peyghambarian, N. *J. Disp. Technol*. **2010**, *6*, 1.